Sustained deposition of contaminants from the *Deepwater Horizon* spill

Beizhan Yan[a,1,2], Uta Passow[b,1,2], Jeffrey P. Chanton[c], Eva-Maria Nöthig[d], Vernon Asper[e], Julia Sweet[b], Masha Pitiranggon[a], Arne Diercks[e], and Dorothy Pak[b]

[a]Lamont-Doherty Earth Observatory of Columbia University, Palisades, NY 10964; [b]Marine Science Institute, University of California, Santa Barbara, CA 93106; [c]Department of Earth, Ocean and Atmospheric Science, Florida State University, Tallahassee, FL 32306; [d]Alfred Wegener Institute, Helmholtz Centre for Polar and Marine Research, D-27570 Bremerhaven, Germany; and [e]Department of Marine Science, The University of Southern Mississippi, Stennis Space Center, MS 39529

Edited by David M. Karl, University of Hawaii, Honolulu, HI, and approved April 26, 2016 (received for review July 4, 2015)

The 2010 *Deepwater Horizon* oil spill resulted in 1.6–2.6 × 10^{10} grams of petrocarbon accumulation on the seafloor. Data from a deep sediment trap, deployed 7.4 km SW of the well between August 2010 and October 2011, disclose that the sinking of spill-associated substances, mediated by marine particles, especially phytoplankton, continued at least 5 mo following the capping of the well. In August/September 2010, an exceptionally large diatom bloom sedimentation event coincided with elevated sinking rates of oil-derived hydrocarbons, black carbon, and two key components of drilling mud, barium and olefins. Barium remained in the water column for months and even entered pelagic food webs. Both saturated and polycyclic aromatic hydrocarbon source indicators corroborate a predominant contribution of crude oil to the sinking hydrocarbons. Cosedimentation with diatoms accumulated contaminants that were dispersed in the water column and transported them downward, where they were concentrated into the upper centimeters of the seafloor, potentially leading to sustained impact on benthic ecosystems.

Deepwater Horizon | oil spill | hydrocarbon | diatom bloom | drilling mud

About 3.2 million barrels of crude oil were released during the *Deepwater Horizon* (DwH) oil spill into the Gulf of Mexico (GoM) between 20 April 2010 and 15 July 2010 (1–4). The spill was extraordinary in its volume, duration, depth of release (~1,500 m), and distance traveled, resulting in hundreds of square kilometers of pollution (5, 6). Roughly 5–10% of the spilled oil reached the seafloor (7–9), although the patchy distribution of this deposition combined with its large spatial extent resulted in significant uncertainty in this estimate (10). This deposition of DwH oil compounds was associated with exceptionally high deposition rates of marine organic and inorganic particles (11). Deposition patterns and type are consistent with the hypothesis that marine snow carried a significant fraction of the deposited oil compounds downward (10, 12), a process dubbed the "Dirty Blizzard."

Marine snow is defined as composite particles > 0.5 mm and consists of phytoplankton, zooplankton feces, feeding structures, mucus, and other debris (13). This material sinks rapidly from the surface ocean (14) and efficiently scavenges suspended or dissolved substances that it encounters (15). By transporting material from the upper to the deep ocean, marine snow acts as a link between the sea surface and the seafloor (16). Different types of marine snow laden with oil (marine oil snow) have been suggested to have transported spilled oil from the surface and from the subsurface plume at ~1,000 m to the seafloor during the DwH spill (17).

Knowledge of the specific fate and distribution pathways of oil and spill-associated chemicals sheds light on the overall ecosystem response to large oil inputs and the transport mechanisms that remove petrocarbon and other contaminants from the water column. Petrocarbon is defined as petroleum and petroleum transformed by weathering processes, including photooxidation and microbial oxidation, burning, or evaporation. Knowledge of petrocarbon fate is important for litigation purposes and future spill response and restoration planning (18). For example, transport of oil-derived carbon to the seafloor was not one of the mechanisms accounted for in the reckoning of the oil spill calculator (1). However, it will likely be taken into account in the future.

Only weeks after the spill had ended, hydrocarbon from the DwH event was largely undetectable in surface waters (19) and in the water column of the GoM [e.g., cruise *Henry Bigelow 02* (14–30 August 2010)]. This may be because their concentrations were below analytical detection limits, or it could have been due to the patchiness of their distribution. We hypothesize (*i*) that petrocarbon and other contaminants lingering in the water column were adsorbed to fine particles and (*ii*) that the downward transport of these materials was controlled by the sedimentation of marine snow. To test these hypotheses, we deployed a funnel-shaped sediment trap [Kiel 21 trap, K.U.M. Umwelt und Meerestechnik Kiel GmbH (KUM)] about 7 km SW of the DwH well (28°42.55'N, 88°25.34'W) at ~1,540 m (Fig. 1), through which the time series of petrochemical sedimentation captured in the sediment trap was examined. This approach allowed us to overcome both analytical limitations and patchiness of distribution because the trap integrated sinking materials over time and space. The second hypothesis was examined by comparing the temporal coherence of pollutant flux with the fluxes of other particles to the deep ocean.

Significance

Despite numerous publications reporting the accumulation of petroleum hydrocarbons associated with the *Deepwater Horizon* spill on the seafloor, the mechanisms of their delivery to the seafloor remain unclear. We demonstrate sedimentation of black carbon derived from the in situ burning of surface oil slicks for about 2 mo following the cessation of burning while other contaminants from the spill, including bioactive barium derived from drilling mud, continued to sediment for at least 5 mo after the well was capped. We also show that the episodic sinking of spill-associated substances was mainly mediated by marine particles, especially diatoms. Together, these data demonstrate delivery mechanisms of contaminants from the spill to benthic ecosystems in the deep Gulf of Mexico.

Author contributions: B.Y. and U.P. designed research; U.P., V.A., and A.D. collected samples; B.Y., U.P., J.P.C., E.-M.N., J.S., M.P., and D.P. conducted lab analyses, B.Y., U.P., and J.P.C. synthesized the data and wrote the paper.

The authors declare no conflict of interest.

This article is a PNAS Direct Submission.

Freely available online through the PNAS open access option.

Data deposition: Data are publicly available through the Gulf of Mexico Research Initiative Information & Data Cooperative (GRIIDC) at https://data.gulfresearchinitiative.org (doi: 10.7266/N7MK69V2, doi: 10.7266/n77942nj, doi: 10.7266/N7BR8Q6H).

[1]B.Y. and U.P. contributed equally to this work.

[2]To whom correspondence may be addressed. Email: yanbz@LDEO.columbia.edu or uta.passow@lifesci.ucsb.edu.

This article contains supporting information online at www.pnas.org/lookup/suppl/doi:10.1073/pnas.1513156113/-/DCSupplemental.

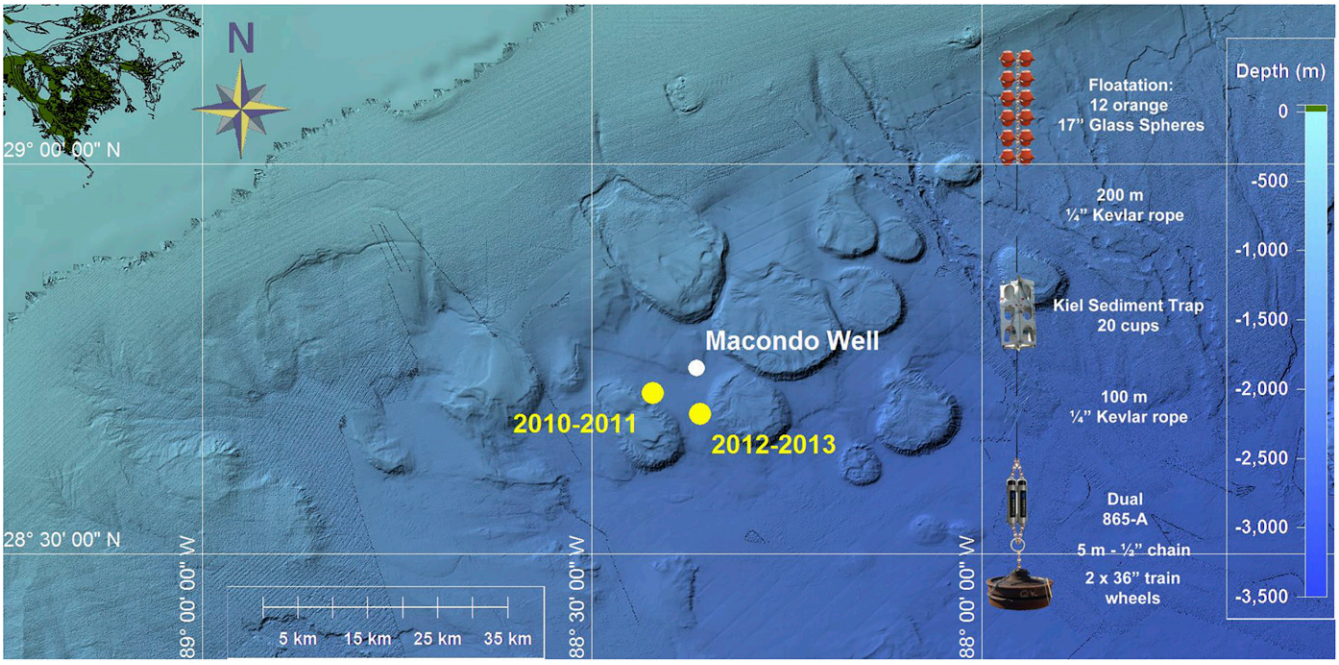

Fig. 1. The sampling site and schematic of sediment trap array deployed in 2010/2011 and 2012/2013, with NOAA *Okeanos Explorer* bathymetry data included.

From analysis of these time series samples, we present conclusive evidence that sedimentation of DwH-associated oil components continued for 5 mo after the damaged Macondo well was capped. Sinking material was collected in 20 consecutive 3-wk intervals between 25 August 2010 and 19 October 2011 and fixed in situ with mercuric chloride in a salinity gradient [40 practical salinity unit (PSU)]. Type and abundance of collected materials are determined by particle dynamics in the region of the source water above the trap. After retrieving the trap, samples were examined microscopically, analyzed for dry mass, particulate organic carbon (POC), petroleum hydrocarbons, barium in different particulate phases, black carbon (BC), δ^{13}C-POC, Δ^{14}C-POC, and δ^{34}S-POM isotopic composition, among other parameters (see *Methods*). Sedimentation patterns in 2010/2011 were compared with those in 2012/2013. This later mooring was deployed about 9 km east of the 2010 trap site (Fig. 1) and collected samples between 28 June 2012 and 22 July 2013.

Results and Discussion

In early September 2010, an exceptionally large sinking event of a *Skeletonema sp.* (diatom) bloom was observed (Table 1) with a sedimentation rate of POC far in excess of sedimentation rates in the fall of 2011 and 2012 (109 mg POC·m^{-2}·d^{-1} vs. ≤20 mg POC·m^{-2}·d^{-1}, Fig. 2 and Fig. S1). During this event, more than 8 billion diatom frustules per square meter per day, dominated by *Skeletonema sp.*, reached 1,500 m depth, carrying with them ~120 μg·m^{-2}·d^{-1} of the sum of *n*-alkanes from C_{22} to C_{36} (ΣSH) and 8.40 mg·m^{-2}·d^{-1} BC, as well as 1.60 mg·m^{-2}·d^{-1} barium and 3.70 μg·m^{-2}·d^{-1} olefins (Table 1 and Table S1). Barite (barium sulfate) and olefin compounds are key components of drilling mud. Aside from this exceptional 2010 fall sedimentation event, annual peak sedimentation rates of POC were observed in spring (2011, 2013) and were about 50% lower than those of the 2010 fall bloom (Fig. 2 and Fig. S1). Peak fluxes of particulate inorganic matter (PIM) and POC in spring reflect seasonality in the discharge of nutrients and suspended minerals by the Mississippi River (Fig. S2). The biological response to this nutrient input is a phytoplankton bloom (20, 21). Sinking marine snow resulting from such blooms incorporates suspended minerals and other nonsinking particles (15, 22), causing seasonal sedimentation pulses as observed in spring 2011 and spring 2013.

In August 2010, an anomaly of MODIS (Moderate Resolution Imaging Spectroradiometer) fluorescence line height, used as a proxy for phytoplankton biomass, was observed in the northeastern GoM, suggesting the occurrence of large phytoplankton blooms related to the DwH spill (21). *Skeletonema sp.,* a common diatom in the GoM, thrives in the presence of crude oil and is known to be associated with oil extraction activities (23). At bloom concentrations, *Skeletonema sp.* coagulates and forms rapidly sinking marine snow aggregates (24), which may be facilitated by the presence of oil and BC. Oil products can promote aggregation and subsequent efficient sedimentation of marine particles (25), because oil-containing aggregates are larger and more cohesive than those formed in the absence of oil (17). In particular, BC from fossil fuel combustion is very surface-active (26) and promotes the coagulation of marine particles (27).

Two BC components (soot and char) can be formed through incomplete combustion. BC sources in the GoM in 2010 include in situ burning (ISB) of crude oil (*Supporting Information*) and atmospheric deposition from boat traffic related to various activities (e.g., skimming). Soot formed in the gas phase from both ISB and boat traffic will be distributed farther afield (28), whereas char, which is the burn residue left on surface waters after ISB, will stay in the water column and be subject to deposition (29). From late April to mid-July, about 400 controlled ISBs were conducted within 24 km of the well (29, 30), removing ~220,000–310,000 barrels of oil (1). Production rates of char, the burn residues, are about 5% (±4%) of the mass of crude oil burned, depending on burn temperature, thickness, and surface area of crude oil on the water surface, etc. (31, 32). Assuming that 5% of burned oil was transformed into char and that all produced char was deposited within 24 km of the well (approximately the area where ISB took place) results in an input of 0.9–1.3 g·m^{-2}. Sedimentation of char in association with the diatom bloom represents 15–20% of this input (see *Supporting Information* for details). After the bloom sedimentation, char concentration

Table 1. Sedimentation rates of dry wt., diatoms, foraminifera, barium, ΣPAH, ΣSH, BC, and the signal of Δ^{14}C-POC and δ^{34}S-POM

Phase	Cup no.	Start date, mm/dd/yy	Dry wt., $mg \cdot m^{-2} \cdot d^{-1}$	Diatom frustules, $10^6\ m^{-2} \cdot d^{-1}$	Foramanifera, $m^{-2} \cdot d^{-1}$	Barium, $mg \cdot m^{-2} \cdot d^{-1}$	ΣPAH, $\mu g \cdot m^{-2} \cdot d^{-1}$	ΣSH $\mu g \cdot m^{-2} \cdot d^{-1}$	BC, $mg \cdot m^{-2} \cdot d^{-1}$	Δ^{14}C-POC, ‰	δ^{34}S-POM, ‰
1	1	8/25/10	1618 ± 160	8135	27	1.60 ± 2.17	0.87 ± 0.12	117.1 ± 13.0	8.42 ± 0.15	−21.4	21.9
2	2	09/15/10	663 ± 46	35	130	0.25 ± 0.02	0.18 ± 0.02	13.2 ± 1.1	0.42 ± 0.08	+76.1	16.7
	3	10/06/10	426 ± 18	62	130	0.26 ± 0.01	0.14 ± 0.02	6.2 ± 0.4	0.31 ± 0.06	−80.9	14.4
	4	10/27/10	519 ± 43	28	140	0.59 ± 0.05	0.19 ± 0.02	42.4 ± 4.1	NA	−113.7	7.5
	5	11/17/10	283 ± 28	14	198	0.22 ± 0.02	0.20 ± 0.03	1.2 ± 0.1	NA	−114.3	8.4
	6	12/08/10	671 ± 15	NA	264	0.43 ± 0.01	0.39 ± 0.04	3.8 ± 0.2	0.44 ± 0.13	−141.0	9.1
3	7	12/29/10	467 ± 16	NA	280	0.22 ± 0.01	0.20 ± 0.02	3.9 ± 0.2	NA	−67.0	5.3
	8	01/19/11	420 ± 24	NA	411	0.17 ± 0.01	0.19 ± 0.02	3.3 ± 0.3	NA	−72.4	4.8
	9	02/09/11	337 ± 20	NA	259	0.17 ± 0.01	0.19 ± 0.02	2.8 ± 0.2	NA	−94.9	2.9
	10	03/02/11	1282 ± 28	3	149	0.70 ± 0.02	0.44 ± 0.05	9.0 ± 0.5	1.07 ± 0.02	−85.1	5.0
	11	03/23/11	746 ± 35	NA	390	0.32 ± 0.02	0.28 ± 0.03	4.3 ± 0.3	NA	−103.2	6.7
	12	04/13/11	763 ± 29	NA	283	0.41 ± 0.02	0.35 ± 0.04	6.7 ± 0.3	NA	−53.8	6.7
	13	05/04/11	248 ± 9	NA	229	0.13 ± 0.01	0.18 ± 0.02	1.7 ± 0.1	NA	−69.9	8.5
	14	05/25/11	762 ± 54	NA	332	0.21 ± 0.02	0.4 ± 0.05	5.9 ± 0.5	NA	−60.1	6.0
	15	06/15/11	440 ± 29	8	381	0.19 ± 0.01	0.23 ± 0.03	2.8 ± 0.2	NA	−20.2	5.1
	16	07/06/11	291 ± 7	NA	276	0.14 ± 0.01	0.16 ± 0.03	0.6 ± 0.1	NA	−20.4	4.4
	17	07/27/11	400 ± 30	NA	300	0.12 ± 0.01	0.20 ± 0.02	2.9 ± 0.3	0.49 ± 0.027	−60.9	12.4
	18	08/17/11	314 ± 50	16	230	0.11 ± 0.02	0.26 ± 0.03	3.0 ± 0.5	NA	−67.9	14.9
	19	09/07/11	384 ± 22	28	155	0.12 ± 0.01	0.56 ± 0.06	0.7 ± 0.1	NA	−56.6	8.6

Phase 1 is the period impacted by diatom bloom, phase 2 represents continued cosedimentation of oil spill associated substances, and phase 3 was when sedimentation of oil spill related substances was negligible; NA, no analysis; ± is the SD; uncertainty of Δ^{14}C-POC is 3.0‰, and δ^{34}S-POM is 0.3‰ based on replicate analysis of randomly selected samples. The Δ^{14}C-POC value of cup 2 is positive. See Table S2 for the list of PAH compounds for calculating ΣPAH.

decreased to background levels (Table S1), indicating a residence time of BC in the water column of about 2 mo, similar to what has been observed elsewhere (33).

The hydrocarbons that sank together with the diatom bloom were predominantly petroleum-derived. The carbon preference index (CPI), which is a mathematical expression of the odd-over-even predominance between n-C_{24} and n-C_{36} (see *Supporting Information* for CPI equation) of the Macondo crude oil is ∼1 (34). In contrast, surface sediments collected from sites unaffected by DwH or natural oil seeps have a CPI of ∼2.5 (*Supporting Information*). A CPI value of about 1.3 in the first sample indicates the dominance of alkanes from crude oil. In addition, the sensitive polycyclic aromatic hydrocarbon (PAH, Table S2) source indicator $C_0/(C_0+C_1)$-P/A (phenanthrene/anthracene), was below 0.5 (35, 36), confirming that crude oil was the dominant source of sinking hydrocarbons in late summer to early fall 2010 (*Supporting Information*). In contrast to the 2010 samples (Fig. 3), the trap samples from 2012 all had a PAH source indicator value of greater than 0.8 (Table S3). A $C_0/(C_0+C_1)$-P/A ratio of 0.5 delineates the transition between unburned (<0.5) and combusted petroleum (>0.5) (36, 37). This indicator is sensitive to weathering of oil as well, because its value decreases as fresh crude oil weathers (38). The decrease causes the difference between weathered crude oil and combustion sources (i.e.,

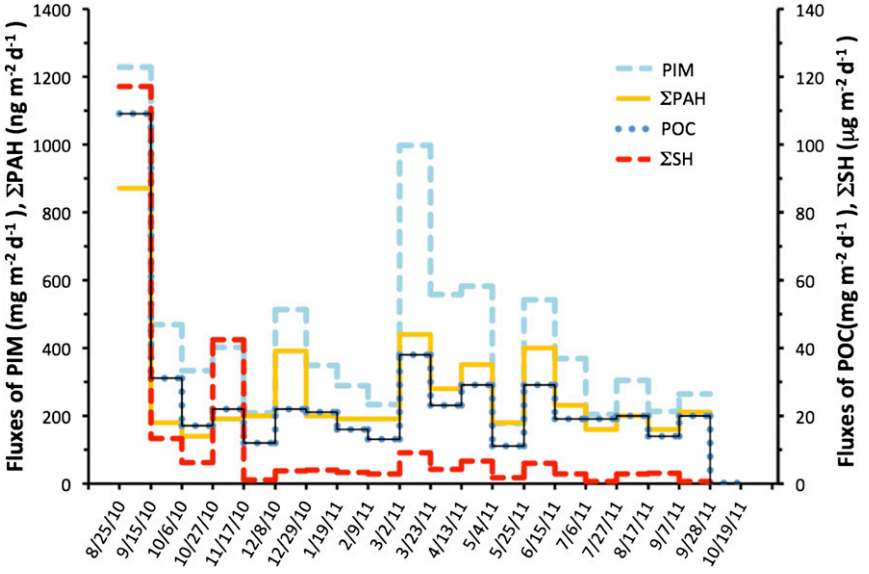

Fig. 2. Temporal change in sedimentation rates of PIM, POC, the sum of saturated hydrocarbons (ΣSH), and the sum of PAHs (ΣPAH). Estimated uncertainties of sedimentation rates are 10%, and uncertainties of PIM, ΣSH, and ΣPAH can be found in Table 1 and Table S1.

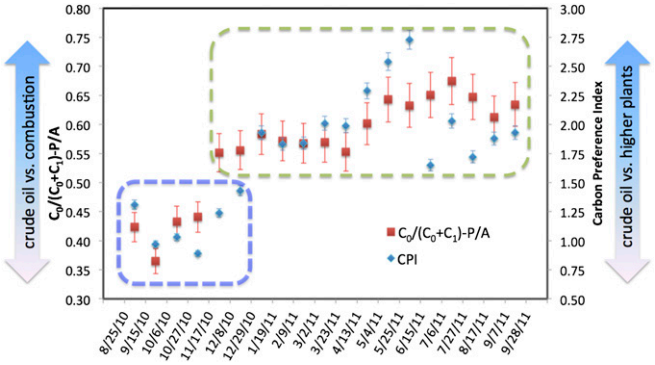

Fig. 3. Relative hydrocarbon contributions from crude oil in settled materials, as revealed by hydrocarbon source indicators. The blue box, in which CPI is <1.6 and $C_0/(C_0+C_1)_{P/A}$ ratio is <0.5, highlights the samples with significant sources from crude oil (petrocarbon), and the green box marks samples with low or negligible contributions from crude oil. The separation into two periods (blue and green boxes) is artificial and may be seen as a conservative estimate for the timespan during which appreciable amounts of oil components from the DwH spill sank. Before December 2010, petrogenic sources dominated; thereafter, noncrude oil hydrocarbon sources (e.g., higher plants for saturated hydrocarbons and combustion for PAHs) dominated.

pyrogenic PAHs) to be more pronounced (i.e., larger) with the passage of time. The ratio of another independent PAH source indicator Fl/(Fl+Py) (where Fl is fluoranthene and Py is pyrene) is about 0.4 in the first sample, below the transition value of 0.5 (36, 39) (*Supporting Information*). This also confirms the dominance of petroleum-derived sources during this period (25 August through 15 September).

The molecular distribution of alkanes can indicate the origin of the settling petroleum hydrocarbons, because lighter oil components (< C_5) dissolved *en route* to the ocean surface (40, 41), and components between C_5 and C_{13} were largely evaporated or degraded (34, 41). The absence of C_{13} and lighter alkanes in our trap samples may thus imply that sinking petroleum hydrocarbons were from the surface rather than from the subsurface plume (7). However, weathering and consumption of lighter alkanes within the deep-sea plume (42) may have a similar effect, and it is thus not possible to unambiguously determine if the petroleum-derived carbon in the trap samples stemmed from the surface or from the deep plume or both. Incorporation of oil into diatom aggregates during their formation has been shown experimentally (17). Scavenging of oil from the deep plume by settling marine snow is another possible mechanism for the inclusion of oil in marine snow. The net effect of removing dispersed or diluted oil from the water and transporting it to the seafloor is the same in both scenarios.

There was no indication that the petroleum hydrocarbons that were collected in the sediment trap stemmed from resuspended sediments from below the trap or from natural seeps. Planktonic foraminifera were observed in settled material during 2010; however, the absence of benthic species indicates the lack of substantial resuspension during this time period (*Supporting Information*). This observation is consistent with physical indicators; resuspension to more than 100 m above the seafloor requires high current speeds, but, between August and December 2010, the northern GoM was free of large storm events [National Hurricane Center, National Oceanic and Atmospheric Administration NOAA)]. Furthermore, resuspended sediments as a single source could not generate the highly varied temporal patterns of SH, PAH, and BC observed in this study. Natural seeps are also unlikely to be the major petroleum hydrocarbon source in these samples. There are no natural seeps identified within 2 km of the trap site, and only three seeps were identified within 5 km. Due to dissolution, evaporation, degradation, mixing, and dispersion, petroleum hydrocarbons from these small seeps were unlikely to be a measurable source of petrocarbon in the trap. In fact, the absence of measurable amounts of petroleum hydrocarbons in 2011 (Fig. 2) and 2012 trap samples (Table S3) emphasizes that the influence of oil from natural seeps was minimal, assuming that natural seepage proceeded at a relatively constant rate.

The petrocarbon detected in the deep sediment trap indicates that these contaminants had lingered in the water for at least 40 d (15 July to 25 August). This can be due to the slow deposition rate of small particles (e.g., clay), to which those petroleum hydrocarbons, especially those > C_{13}, adsorb due to their low solubility (43). In the open sea, fine suspended particulate matter settles very slowly (<0.01 $mm \cdot s^{-1}$) (44) and thus remains in the surface layers for extended time periods (45, 46). However, those particles can be scavenged by marine snow consisting of diatoms, feces, feeding structures, or detritus, therewith cosedimenting rapidly (47, 48). Marine snow can settle at 50 to >200 $m \cdot d^{-1}$ (12, 14).

The blizzard of sinking diatom aggregates sedimented not only petroleum hydrocarbons but also components of the drilling mud, as indicated by the high fluxes of barium and olefins (Table 1 and Fig. 4). Water-based drilling mud, which contains barite, olefins, and clay bentonite, was used during the DwH event for "top kill" and "static kill" techniques. The molecular distribution of olefin compounds enriched in our trap samples before December 2010 (Table S1 and Fig. 4) exhibited a dominance of C_{16} and C_{18} (Fig. 5), identified by the 2D gas chromatograph (GC×GC) time-of-flight (TOF) mass spectrometer, which unambiguously traces olefins stemming from drilling mud (49, 50). These olefins fell below the detection limit in 2011. When water-based drilling mud is released into the marine environment, the majority of mud solids form a plume that settles quickly to the seafloor, but ~10% of its mass, especially the fine clay and barite particles, remains suspended and disperses (51). Clay, such as bentonite, has a high adsorption capacity for hydrocarbons (52); thus it is reasonable to assume that olefins would adsorb to these clay particles. Due to their extremely low solubility, olefins remain associated with the clay particles after the release of the drilling mud into the water. Similar to other small particles, clay particles likely remained suspended in the water for weeks to

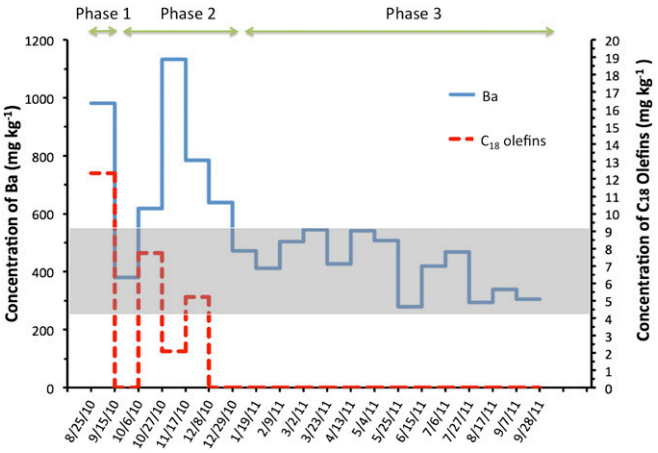

Fig. 4. Concentrations of barium and olefin, two drilling mud-related chemicals, in settled materials. The gray area depicts background concentration for barium in the northern GoM. See Table 1 for definition of three phases. Uncertainties of barium and olefin can be found in Table 1 and Table S1.

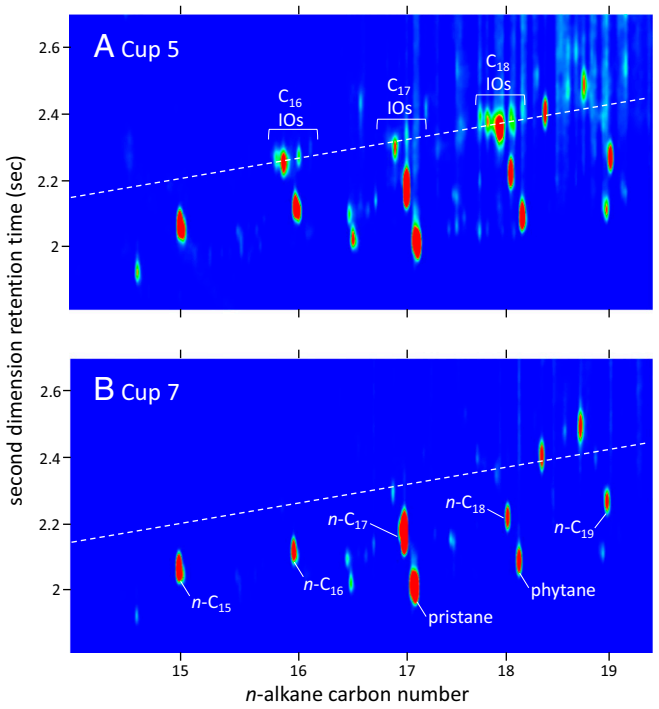

Fig. 5. Partial GC×GC TOF chromatograms of ions of alkene (55 + 69 + 83) in (*A*) cup 5 and (*B*) cup 7, in which data are displayed in color contour plots, with blue, yellow, and red representing low, medium, and high signal strength, respectively. The isomer mixture and pattern of C_{16} to C_{18} internal olefins (IOs) indicates that drilling-mud olefins are present in cup 5 but not in cup 7.

months, until the occurrence of a large sedimentation event (e.g., diatom bloom) transferred them to the seafloor.

An anomaly of dissolved barium, attributed to drilling mud application, was observed in late May at ∼1,100 m depth in the water column about 6.3 km southwest of the well (53), but it is unexpected that high fluxes of barium arrived in the sediment trap in September as far away as 7.5 km from the well site. Due to its high density, barite ($BaSO_4$) was assumed to have sedimented quickly and remain near the application sites (51). In trap material, however, barium was consistently enriched until January 2011, suggesting that sinking marine snow collected barium from the water for up to 4 mo after drilling mud was last used (August). After January, barium concentrations fell to background levels (*Supporting Information*). These unexpected elevated fluxes of barium in trap samples were partially due to the existence of fine barite particles in drilling mud. Electron microprobe analysis confirmed such fine barite particles dominated in cup 1 but not in cup 14 (Fig. S3). Barite particles < 5 μm comprise about 10% of 4.1 specific gravity grade barite (54). Elevated barium flux during the sedimentation of the diatom bloom was also due to barium associated with the Al–Si phase, which includes both clay and biologically produced opal frustules (*Supporting Information*).

In addition, barium was incorporated into biogenic particles, extending its residence time in the water as well. Using a sequential leaching approach modified from Eagle et al. (55, 56), we found that the Ba:Ca ratio in the carbonate phase in cup 1 is ∼3 times that in cup 14, implying the incorporation of extra Ba into calcium carbonate tests and shells (*Supporting Information*). The Ba:Ca ratios in planktonic shells are correlated with the Ba levels in the water (57, 58). Our results suggest that the application of barite in drilling mud can increase the dissolved barium concentration in the water, leading to its increased incorporation into planktonic shells (e.g., foraminifera and pteropods). Considering the widespread use of drilling mud at hundreds of ocean drilling sites around the world, the environmental implications (59, 60) of such an unexpectedly long residence time of barium in the water column is significant and worthy of further investigation.

The concurrence of elevated sedimentation rates of drilling mud components and oil products, including petroleum hydrocarbons and BC, with diatoms (POC, diatom abundance) suggests that rapidly sinking diatom aggregates scavenged suspended substances and particles from the spill and mediating measures, effectively cleansing the water column. Cosedimentation of petrocarbons with organic matter has been observed under nonspill conditions as well (47, 48, 61, 62). The presence of fresh marine phytoplankton during the bloom sedimentation is indicated by intact cells, the modern Δ^{14}C-POC signature, which reflects the relative contributions of crude oil and modern carbon (e.g., phytoplankton), and in the marine source signatures of δ^{34}S-POM and δ^{13}C-POC (Table 1 and Table S1).

The mass sedimentation event in early September 2010 was followed by a temporary decrease in the sedimentation of oil and drilling mud markers between mid-September and October (Table 1). Despite the persistent low rates of POC and PIM sedimentation until March 2011 (Fig. 2), sedimentation of DwH-related substances (e.g., barium, olefins, and ΣSH) increased again in late October 2010 (Fig. 4). Additionally, the relative contributions of the spill-related substances to total settled material were transiently low directly after the mass sedimentation event. For example, the barium contribution to sinking material decreased from about 1,000 mg·kg^{-1} of dry weight during the bloom sedimentation event to 400 mg·kg^{-1} directly thereafter (Fig. 4), but then rebounded to about 1,200 mg·kg^{-1} in late October. We hypothesize that the short-lived decrease in the relative contribution of barium to total sinking matter immediately after the mass sedimentation event reflected a transient decrease of barium concentration in the water column near the trap caused by the "scrubbing effect" of the large diatom flux event. However, diatom blooms are spatially patchy (21), and lateral advection and mixing of polluted waters that did not experience a diatom bloom, as well as an influx of organisms with Ba-rich shells, would have led to the renewed increase in concentrations of the spill-related contaminants in late October.

The Δ^{14}C-POC signal is consistent with a transitory variation in the contribution of oil spill contaminants to sinking matter directly after the fall bloom (Fig. S4): During the diatom sedimentation event (phase 1, see Table 1), the fossil fuel signal was masked by the large amount of newly assimilated phytoplankton carbon that sank, resulting in a more modern overall value (Δ^{14}C-POC = −21‰). The Δ^{14}C-POC signal increased further (+76‰) in the second half of September 2010, as fossil carbon (Fig. S4) was temporarily cleansed from the water column, but phytoplankton still sank, albeit at low concentrations (Table 1). A value of +40‰ or greater is indicative of modern carbon fixed at the surface (63). The subsequent rapid shift to Δ^{14}C-POC representing more fossil carbon in October (−80‰) to the end of December (−140‰), reflects the renewed increase in the relative contribution of oil components to total settled material, as oil constituents increased again in source water (phase 2). In 2011, Δ^{14}C-POC became successively more modern and trended with the PAH source indicator ($C_0/(C_0+C_1)$-P/A), as contributions of crude oil to total organic carbon flux and to petroleum hydrocarbons simultaneously decreased with time (Fig. S4, phase 3). The δ^{34}S-POM values of +14‰ to +21‰ confirmed initial algal inputs and then declined to values below +10‰ as these became less prominent, consistent with the dynamics suggested by Δ^{14}C-POC data (Table 1).

Scavenging and subsequent sedimentation of oil-spill-related substances is not only determined by their concentrations in the water but also by their respective physicochemical characteristics, including their affinities to sinking particles. As an example,

sedimentation rates of BC, which is highly surface-active, declined first, in September, whereas sinking crude oil-derived hydrocarbons declined by late December 2010. Although olefins and barium both stemmed from the same source, olefin sedimentation declined earlier than barium, which was incorporated into planktonic shells. The observed temporal sequence of loss of oil spill contaminants in sinking matter is consistent with the interpretation that these substances all originated from a single event, the DwH oil spill.

After mid-January 2011, no unequivocal sedimentation of oil-spill-related substances was observed. PAH and SH continued to sediment, but the source indicators used suggest that they were predominately derived from noncrude oil sources (e.g., riverine input). The CPI and $C_0/(C_0+C_1)$-P/A ratios exceeded 1.7 and 0.55, respectively, similar to values observed in the trap in summer 2012 (Table S3) and in sediments at a reference site that was not impacted by the spill or by natural oil seeps. Principal component analysis based on hopane and sterane biomarker ratios also confirmed that those 2011 trap samples were distinctly different from the Macondo oil (Fig. S5 and Table S4). Olefins were absent and sedimentation of barium declined to background levels, as those found in unaffected sediments in the northern GoM (64). $\Delta PO^{14}C$, although variable, possibly due to riverine input (65–67), remained around −90‰ to −50‰, indicating greater relative importance of modern carbon with less fossil input (*Supporting Information*).

About 2,272 $\mu g \cdot m^{-2}$ ΣSH sank in excess of background values between late August and December 2010, equivalent to the downward transport of about 85 (±7.04) $mg \cdot m^{-2}$ of crude oil (*Supporting Information*). Assuming a petrocarbon footprint of 8,400 km^2 (8), the ΣSH sedimentation between late August and December 2010 was about 7.2 (± 0.6) × 10^8 grams, which is ∼0.14 (± 0.01)% of the total amount of crude oil released, and 0.8–8.1% of petrocarbon flux to the seafloor estimated by Chanton et al. (8) using ^{14}C data in surface sediments, and 0.7–6% of the flux estimated by Valentine et al. (7) (see *Supporting Information* for details of the estimation). The fact that sedimentation of a single diatom bloom at a time when oil concentrations in the water were considered negligible carried to depth on the order of 5% of the sunken oil compounds suggests that just a few marine snow sedimentation events during and after the spill could easily explain the observed deposition of oil and marine particles to the seafloor.

In conclusion, the persistent deposition of the spill-associated substances in the 5 mo after the spill is evidence that oil spill and drilling mud-derived substances must have lingered in the water column long after their release ended, although oil visible at the sea surface disappeared within weeks following capping (19). Barium remained in the water column for months and even entered pelagic food webs. The sedimentation of these spill-related substances was mediated by marine snow, specifically, by a diatom bloom. The oil and BC likely promoted aggregation of marine particles, leading to more effective sedimentation and the resultant transport of exceptionally large amounts of oil-derived material, some 1.6–2.6 × 10^{10} g (8), to the seafloor. Scavenging of these substances from the water column by sinking marine snow provides a mechanism for previously dispersed oil to reaccumulate at the seafloor. These same mechanisms must have been in effect before the leak was capped, leading to unprecedented accumulation rates at the seafloor and providing an explanation for DwH's unexpectedly strong impacts on benthic organisms, including fish and coral in deep waters (68–71).

Methods

Site Description and Sampling Method. The trap was moored at 28°42.55′N, 88°25.34′W in 1,538 m water depth about 105 m above the seafloor. This site was chosen for its proximity to the DwH well head (∼7.4 km SW) and because it positioned the trap under the subsurface plume observed at around a 1,000-m depth to the southwest of the incident site. The deployment site is characterized by a smooth flat bottom of mostly muddy sediments located to the west of Gloria Dome and just to the east on the NE side of Biloxi Dome. For comparison, data from a deployment at 28°40.78′N, 88°21.68′W, about 5 nautical miles east of the initial trap sites (Fig. 1) in 1,655 m water depth and about 80 m above the seafloor, were analyzed. Settling material was collected in four consecutive cups between 28 June 2012 and 8 September 2012 as well as in 18 cups between 12 September 2012 and 22 July 2013. Bathymetry data in Fig. 1 are from NOAA Okeanos Explorer cruises EX1105, EX1202L2, and EX1202L3 and from the General Bathymetric Chart of the Oceans.

The opening of the almost 2-m-high funnel-shaped Kiel Sediment trap (KUM; www.kum-kiel.de/home/) has a 0.5-m^2 collection surface, which is covered with a hexagonal lattice grid baffle that reduces washout. The multibottle turntable allows for the collection of 20 individual samples in 300-mL polypropylene bottles. Samples were collected over 21-d intervals between 25 August 2010 and 19 October 2011. Before deployment, sample bottles were filled with filtered seawater to which NaCl (pro analysis, Fisher Scientific) was added to a final salinity of ∼40 PSU and the preservative $HgCl_2$ at a final concentration of ∼0.14%. Upon retrieval, cups were stored and transported dark and cold (4 °C) until processing and analysis. First, cups were gently mixed, and, after material was allowed to resettle for 7 d, sample material was split repeatedly using a Folsom Plankton splitter. During splitting, artificial seawater was used for rinsing. One 1/8 split was used for hydrocarbon analysis, 1/16 split was used for isotope measurements, and appropriate fractions of 1/128 splits were used for the determination of dry weight, POC, barium, and microscopical enumeration of phytoplankton and foraminifera. On average, dry weight measurements between different splits varied by <6%. Depending on analysis, split samples were transferred into appropriate containers, e.g., precombusted glass bottles (at 450 °C overnight) for hydrocarbon analysis. Due to the unexpected nature of the spill, only one trap was deployed. Sedimentation rates in 2012–2013, which are presented for comparison, were measured with a similar time series sediment trap, a funnel-shaped McLane trap moored at 28°40.78′N, 88°21.68′W. Sample processing and analysis were generally the same as for the first 2010/2011 trap.

Analysis.

Dry weight, PIM, and POC. Quadruplicate sample aliquots were filtered onto preweighed and precombusted (450 °C for 4–6 h) 25-mm glass microfiber filters (GF/F), briefly rinsed with Milli-Q (MQ) water, and dried at 60 °C before reweighing for dry weight determination (dry wt.). PIM was determined from one duplicate set of dry wt. filters, reweighing a third time after combustion at 450 °C for 4–6 h to remove organic matter. The filters for determination of POC were fumed with 10% HCl to remove inorganic carbon and analyzed using a carbon, hydrogen, nitrogen (CHN) elemental analyzer (model C 44OHA by Control Equipment, now Exeter Analytical).

Isotopes. Before carbon isotope analysis, samples were dried, ground, treated with 10% HCl to remove carbonates, rinsed, and freeze-dried. Samples were then analyzed for percent organic carbon (%C), $\delta^{13}C$-POC, and $\Delta^{14}C$-POC. The first two analyses were performed on a Carlo Erba elemental analyzer coupled to a Delta XP Thermo Finnegan isotope ratio mass spectrometer. Results are presented relative to Vienna Pee Dee Belemnite (VPDB) [$\delta^{13}C = (R_{sam}/R_{std} - 1) \times 1{,}000$, where $R = {}^{13}C/{}^{12}C$]. Samples for $\Delta^{14}C$-POC analysis were combusted (72) and purified CO_2 prepared as graphite targets were analyzed by accelerator mass spectrometry at the University of Georgia (UGA) Center for Applied Isotope Studies (73). Values are reported according to the Δ notation put forth in ref. 74. The Δ notation normalizes the radiocarbon content of a sample to a nominal $\delta^{13}C$ value (−25‰) and the year that the sample was collected. The scale is linear and starts at −1,000‰ when a sample has essentially 0% modern carbon, which would represent petroleum residue (75, 76). Analytical reproducibility was on the order of 3‰. The $\Delta^{14}C$ content of dissolved inorganic carbon in the open Gulf was +41 ± 3‰ (63). Plankton in 2010 and 2011 was +23 ± 20‰. The greater variability in the plankton was due to the admixture of fossil carbon, the same thing we are measuring here. Measurement variability is small relative to the signal we are measuring. In parallel, $\delta^{13}C$-POC was also determined in a CHN elemental analyzer (Finnigan Delta Plus Advantage) from subsamples processed as for POC (filtering onto precombusted 25-mm GF/F filters and fuming these with 10% HCl). Results from both $\delta^{13}C$-POC determinations agreed well, and averages were used.

Samples for sulfur isotope analysis ($\delta^{34}S$-POM) were first combusted with an elemental analyzer (S 4010). SO_2 gases were separated with a 0.8-m GC column (100 °C) and analyzed with a continuous flow isotope ratio mass spectrometer (Delta Plus XP) (77). Final determination of ^{34}S-POM was based

on ions 64 and 66, using a dial reactor configuration (78) with the second reactor full of quartz chips to buffer ^{18}O contribution to the SO_2. Approximately 5 mg of niobium pentoxide was amended to each sample to improve combustion. No correction for oxygen isotope contribution was made. At least three isotopic reference materials were interspersed with samples for calibration. Sulfur isotopic ratios are reported in per mill relative to Vienna Canyon Diablo Troilite (VCDT) by assigning a value of −0.3 per mill to International Atomic Energy Agency (IAEA) S-1 silver sulfide (79).

The sequential leaching experiment. We conducted a sequential leaching analysis for trap samples 1 and 14, following an approach modified from Gonneea and Paytan (56). Five steps are listed as follows: (*i*) 13 mL 4N acetic acid was added to 0.5–1 g of samples, and samples were then shaken overnight; (*ii*) 13 mL of 10% (wt/wt) sodium hypochlorite was added, and then the samples were placed in a 50 °C water bath overnight; (*iii*) 13 mL of 0.2 N hydroxylamine in 25% acetic acid was added, and the samples were placed in 80 °C water bath overnight; (*iv*) 12 mL of 1:2 40% hydrofluoric acid (HF):1 N nitric acid was then added and shaken overnight; (*v*) samples were heated to ∼230 °C and dried down to small volume, and then nitric acid, perchloric acid, and concentrated HF were added. The walls were washed down with nitric acid, followed by addition of 2.5 mL of 5% boric acid (wt/vol, aqueous) and then 7 mL MQ water. Between each step, samples were rinsed three times with 5 mL water. The water from the three rinses after each step was combined. Inductively coupled plasma mass spectrometry (ICP-MS) was used to measure barium and calcium levels, after dilution where necessary. The trap 1 sample and a GoM sediment sample were analyzed twice to evaluate the uncertainties of this method. The results of the repeated measures for total barium levels are consistent (±6%), and values of the National Institute of Standards and Technology (NIST) 1643e standard are within 1% of the certified amount.

Measurement of total Ba level in all trap samples. For measuring the total Ba level in trap samples, about 10 mg of material was filtered onto 0.6-μm polycarbonate (PC) filters (47 mm) that had been prerinsed with, first, 40 mL of 10% HCL and, then, 200 mL of MQ water. Samples were digested using 0.5 mL concentrated HNO_3 (Seastar Baseline) + 0.3 mL HF (Ultrex) + 0.2 mL H_2O_2 (ACS reagent grade). Samples were microwaved in sealed Teflon containers for 5 min, cooled, and then microwaved another 5 min. Next, 2.4 mL of 5% boric acid (ACS reagent grade) was added, and the sample was microwaved for another 5 min. On cooling, the samples were diluted 20× in 1% HNO_3 and analyzed for Ba, Al, and Fe using a Thermo Fisher Element 2 ICP-MS operated in medium resolution. Calibration was by external standards, and 2 ppb In was added to the diluted samples as an internal standard.

Phytoplankton and foraminifera enumeration. Subsamples were investigated using an inverted microscope (IM 35; Zeiss) according to the Utermöhl method (80). A minimum of 50–100 phytoplankton cells of the dominant groups were enumerated at four magnifications (100×, 160×, 250×, and 400×) using phase contrast microscopy. Only the dominant, identifiable cells were considered; for diatoms, intact cells (plasma containing frustules), empty frustules, and resting spores were counted separately. Totals are presented.

Planktonic foraminifera were picked wet from 1/16 or 1/32 splits after wet sieving at 100 μm. All foraminifera were picked with a micropipette, speciated, and counted. Total numbers of foraminifera counted per sample ranged from 9 (August 25 sample, 1/32 split) to 270 (January 11 sample, 1/16 split), with an average of 154 foraminifera per sample.

Analysis for hydrocarbons and olefins. Trap sediments and overlaying water fixed with $HgCl_2$ were transferred to plastic centrifuge containers and centrifuged at 3,400 × *g* for 10 min. Water was decanted, and the sediments were transferred to ashed aluminum trays and then dried in an oven at 40 °C under a flow of air filtered through Florisil until dryness. Dry sediments were weighed, ground, and then extracted using 70:30 dimethyl chloride:methanol by Accelerated Solvent Extraction system 200 (ASE 200; previously Dionex, now Thermo Fisher). Six hundred nanogram 17β(H),21β(H)-Hopane (catalog no. 07562; Sigma Aldrich) was added to the extraction cell before extraction. Extracts were evaporated to about 1 mL under a gentle flow of N_2, then an alumina gel liquid chromatograph column was used to purify hydrocarbons (39). Samples were concentrated to ∼200 mL, and then transferred to GC vials and spiked with 0.5 ppm deuterated PAH standard mix, which consists of five separate standards: Acenaphthylene-D8 (catalog no. DLM-2204–1.2; Cambridge Isotope Labs), Indeno[1,2,3-cd]pyrene-D12 (catalog no. DLM-2148–1.2; Cambridge Isotope Labs), Benzo[a]pyrene-D12 (catalog no. S-431; SPEX), Anthracene-D10 (catalog no. 48863; Supelco), and Terphenyl-D14 (catalog no. 48418; Supelco).

Saturated hydrocarbon and olefins analyses were performed on a comprehensive GC×GC TOF mass spectrometer (LECO): An Rxi-1ms column (20 m length, 0.18 mm i.d., 0.18-μm film thickness; Restek) was used in the first dimension, and a BPX50 column (1 m length, 0.1 mm i.d., 0.1-μm film thickness; SGE) was used in the second dimension (49). Primary oven temperature was held at 60 °C for 12 min and then ramped from 60 °C to 350 °C at 1.5 °C·min^{-1}. The secondary oven was set to be 30 °C hotter than the primary oven, and the modulator was set to be 55 °C hotter than the primary oven. The TOF detector signal was sampled at a data acquisition rate of 200 spectra per second. The transfer line was held at a constant temperature of 310 °C, and the source temperature was set at 200 °C. The detector voltage was 1,677 V, the mass scan range was 50–300 amu, and electron energy was 70 eV. Front inlet temperature was 300 °C, initially splitless and then changed to a split ratio of 20:1. The carrier flow was constant at 1.5 mL·min^{-1}.

PAH analysis was performed on a Varian GC-MS (now Agilent) with an option of large volume injection to achieve a lower detection limit. An Rxi-5ms column (30 m length, 0.25 mm i.d., 0.25-μm film thickness; Restek) was installed, and the column oven was held at 50 °C for 5 min, then ramped to 310 °C at 10 °C·min^{-1}, then held at 310 °C for 20 min. The front inlet with ability of cryofocusing was programmed to hold at 20 °C for 0.6 min, ramp to 50 °C at 200 °C·min^{-1}, and hold at 50 °C for 0.6 min, then ramp to 300 °C at 200 °C·min^{-1}, where it remained for the rest of the run. The injector was initially split at a ratio of 20:1, splitless at 1.45 min until 4.25 min when the split ratio was increased to 100:1, finally settling at a split of 20:1 at 7.6 min. A constant carrier flow of 1 mL·min^{-1} was used. The transfer line temperature was 310 °C, the source temperature was 150 °C, and electron energy was 70 eV; 20 μL of each sample was injected per run.

To obtain a reliable and accurate result, quality assurance/quality control was implemented throughout the analysis of organics. Known levels of stable-isotope-labeled internal standards were added to calculate the possible loss of low-molecular-weight hydrocarbons during the purification and concentration steps before analysis. The calibration standards were measured at the beginning and the end of the actual sample measurements. Internal standards were also added to monitor instrument precision. For every 12 samples, NIST standard reference material (SRM) 1648 was processed and analyzed in a manner identical to the trap samples. Only results that fell within certified values were accepted. Recovery rate of low molecular weight hydrocarbons, e.g., naphthalene, was about 50–70%, and recovery of high molecular weight (HMW) hydrocarbons, e.g., chrysene, was 85–115%.

BC analysis. BC was determined using the Interagency Monitoring of Protected Visual Environments (IMPROVE) protocol (81–83). There is no universally accepted method for measurements of BC in ocean sediment samples (84). The method used here has the advantage of determining levels of both char and soot, which are two BC components. The chemothermal oxidation pretreatment (CTO)-375 method (85), which has frequently been used for marine particles and sediments, includes only analysis of soot, not char. We compared our methods and CTO-375 and found that soot levels determined with both methods significantly correlated ($R = 0.84$, $P < 0.01$) (86).

About 150 ± 30 mg ground (<63 μm) and homogenized samples were weighed for acid pretreatments (81, 82). In brief, hydrochloric acid (HCl), HF, and their mixture were used to remove carbonate, metal oxides, and minerals. The remaining residues were filtered through a 47-mm quartz filter (0.4-μm pore size; Whatman) and air-dried in a baking oven at 35 °C. A 0.526-cm^2 circular punch from the filters was stepwise heated to 120 °C, 250 °C, 450 °C, and 550 °C in a pure helium environment, and four organic carbon (OC) fractions were produced: OC1, OC2, OC3, and OC4. Then the oven temperature was raised to 550 °C, 700 °C, and 800 °C in a 2% O_2/98% He atmosphere, and three elemental carbon (EC) fractions were produced: EC1, EC2, and EC3. In this procedure, the pyrolyzed organic carbon produced in the inert He atmosphere was monitored using a laser to determine the OC/EC split. The IMPROVE protocol defines the sum of all three elemental carbon (EC) fractions minus pyrolyzed organic carbon as BC. EC1 minus pyrolyzed organic carbon was defined as char, and the sum of EC2 and EC3 was defined as soot (87).

Electron microprobe analysis of barite particles. To examine the particle size and morphology of barite particles, a small fraction of the residue phase samples from the sequential leaching experiment in cup 1 and cup 14 were subjected to electron microprobe (Cameca SX-100) analysis at Rensselaer Polytechnic Institute. Processed sediments were observed by backscattered electron (BSE) imaging, which indicates the material's electron density where image brightness is proportional to mean atomic number. Processed sediments were placed on carbon tape and coated with ∼20 nm of carbon for electrical conductivity. Electron column conditions included 15 keV accelerating voltage and 1-nanoamp beam current, using the 70-μm aperture. Images were acquired with a single 25-s frame time in scanning mode. Barite appears bright white near saturation in BSE images due to the very high electron density of barium.

ACKNOWLEDGMENTS. The deployment of sediment trap could not be performed without the help of several people, including U. Bathmann and G. Rohard (Alfred Wegener Institute), T. Kumbier (K.U.M. Umwelt und Meerestechnik), Joe Montoya (Georgia Institute of Technology), and the crew of RV *Oceanus*. We also thank Drs. Yongming Han (Chinese Academy of Sciences), Alan Shiller (University of Southern Mississippi), Benjamin Harlow (Washington State University), James Ross (LDEO), Jared Singer (RPI), Samantha Bosman (Florida State University), and Alexander Cherkinsky (UGA Center for Applied Isotope Studies) for careful analysis of samples. Previous versions of the manuscript were improved by comments from Andrew Juhl (LDEO) and Charles Fisher (Pennsylvania State University). The sample collection was funded by two National Science Foundation Rapid projects (OCE-1045330 and 1059103), and the lab analyses was funded by a grant from the Gulf of Mexico Research Initiative to support the "Ecosystem Impacts of Oil and Gas Inputs to the Gulf (ECOGIG)" consortium. Funding was also provided by the National Institute of Environmental Health Sciences Center for Environmental Health in northern Manhattan (p30 ES009089) to establish the Trace Organic lab at LDEO. This is ECOGIG Contribution 441 and LDEO Contribution 8010.

1. Federal Interagency Solutions Group (2010) *Oil Budget Calculator: Deepwater Horizon-Technical Documentation* (Fed Interagency Solutions Group, Washington, DC).
2. McNutt MK, et al. (2012) Review of flow rate estimates of the *Deepwater Horizon* oil spill. *Proc Natl Acad Sci USA* 109(50):20260–20267.
3. Joye SB, MacDonald IR, Leifer I, Asper V (2011) Magnitude and oxidation potential of hydrocarbon gases released from the BP oil well blowout. *Nat Geosci* 4(3):160–164.
4. Malakoff D (January 15, 2015) After geoscientists joust, judge rules BP Gulf spill totaled 3.19 million barrels of oil. *Science*. Available at www.sciencemag.org/news/2015/01/after-geoscientists-joust-judge-rules-bp-gulf-spill-totaled-319-million-barrels-oil. Accessed May 18, 2016.
5. Camilli R, et al. (2010) Tracking hydrocarbon plume transport and biodegradation at Deepwater Horizon. *Science* 330(6001):201–204.
6. Spier C, Stringfellow WT, Hazen TC, Conrad M (2013) Distribution of hydrocarbons released during the 2010 MC252 oil spill in deep offshore waters. *Environ Pollut* 173:224–230.
7. Valentine DL, et al. (2014) Fallout plume of submerged oil from *Deepwater Horizon*. *Proc Natl Acad Sci USA* 111(45):15906–15911.
8. Chanton J, et al. (2015) Using natural abundance radiocarbon to trace the flux of petrocarbon to the seafloor following the *Deepwater Horizon* oil spill. *Environ Sci Technol* 49(2):847–854.
9. Prouty NG, et al. (2016) Impact of *Deepwater Horizon* spill on food supply to deep-sea benthos communities. *Estuarine Coastal Shelf Sci* 169:248–264.
10. Daly KL, Passow U, Chanton J, Hollander D (February 2, 2016) Assessing the impacts of oil-associated marine snow formation and sedimentation during and after the Deepwater Horizon oil spill *Anthropocene*, 10.1016/j.ancene.2016.01.006.
11. Brooks GR, et al. (2015) Sedimentation pulse in the NE Gulf of Mexico following the 2010 DWH blowout. *PLoS One* 10(7):e0132341.
12. Passow U, Ziervogel K, Asper V, Diercks A (2012) Marine snow formation in the aftermath of the Deepwater Horizon oil spill in the Gulf of Mexico. *Environ Res Lett* 7(3):035301.
13. Alldredge AL, Silver MW (1988) Characteristics, dynamics and significance of marine snow. *Prog Oceanogr* 20(1):41–82.
14. Asper VL (1987) Measuring the flux and sinking speed of marine snow aggregates. *Deep Sea Res Part A* 34(1):1–17.
15. Smetacek V (1985) Role of sinking in diatom life-history cycles: Ecological, evolutionary and geological significance. *Mar Biol* 84(3):239–251.
16. Asper VL, Deuser W, Knauer G, Lohrenz S (1992) Rapid coupling of sinking particle fluxes between surface and deep ocean waters. *Nature* 357:670–672.
17. Passow U (October 2014) Formation of rapidly-sinking, oil-associated marine snow. *Deep Sea Research Part II: Topical Studies in Oceanography*, 10.1016/j.dsr2.2014.10.001.
18. Peterson CH, et al. (2012) A tale of two spills: Novel science and policy implications of an emerging new oil spill model. *Bioscience* 62(5):461–469.
19. Gillis J, Robertson C (July 27, 2010) On the surface, gulf oil spill is vanishing fast; *New York Times*, p A1.
20. Turner RE, Rabalais NN (1994) Coastal eutrophication near the Mississippi River delta. *Nature* 368(6472):619–621.
21. Hu C, et al. (2011) Did The northeastern Gulf of Mexico become greener after the *Deepwater Horizon* oil spill? *Geophys Res Lett* 38(9):L09601.
22. Hamm CE (2002) Interactive aggregation and sedimentation of diatoms and clay-sized lithogenic material. *Limnol Oceanogr* 47(6):1790–1795.
23. Parsons ML, Turner RE, Overton EB (2014) Sediment-preserved diatom assemblages can distinguish a petroleum activity signal separately from the nutrient signal of the Mississippi River in coastal Louisiana. *Mar Pollut Bull* 85(1):164–171.
24. Kiorboe T, Lundsgaard C, Olesen M, Hansen JLS (1994) Aggregation and sedimentation processes during a spring phytoplankton bloom—A field experiment to test coagulation theory. *J Mar Res* 52(2):297–323.
25. Muschenheim DK, Lee K (2002) Removal of oil from the sea surface through particulate interactions: Review and prospectus. *Spill Sci Technol Bull* 8(1):9–18.
26. Koelmans AA, et al. (2006) Black carbon: The reverse of its dark side. *Chemosphere* 63(3):365–377.
27. Mari X, et al. (2014) Effects of soot deposition on particle dynamics and microbial processes in marine surface waters. *Global Biogeochem Cycles* 28(7):662–678.
28. Perring AE, et al. (2011) Characteristics of black carbon aerosol from a surface oil burn during the *Deepwater Horizon* oil spill. *Geophys Res Lett* 38(17):L17809.
29. Allen AA, Jaeger D, Mabile NJ, Costanzo D (2011) The use of controlled burning during the Gulf of Mexico *Deepwater Horizon* MC-252 oil spill response. *Int Oil Spill Conf Proc* 2011(1):abs194.
30. Mabile N (2012) The coming of age of controlled in-situ burning. *Proceedings of the 2012 Interspill Conference and Exhibition* (Interspill Ltd, Poole, UK).
31. API (2005) *A Decision-Maker's Guide To In-Situ Burning* (Am Petrol Inst, Washington, DC), Publ no 4740.
32. Buist I (2003) Window-of-opportunity for in situ burning. *Spill Sci Technol Bull* 8(4):341–346.
33. Flores-Cervantes DX, Plata DL, MacFarlane JK, Reddy CM, Gschwend PM (2009) Black carbon in marine particulate organic carbon: Inputs and cycling of highly recalcitrant organic carbon in the Gulf of Maine. *Mar Chem* 113(3–4):172–181.
34. Aeppli C, et al. (2012) Oil weathering after the *Deepwater Horizon* disaster led to the formation of oxygenated residues. *Environ Sci Technol* 46(16):8799–8807.
35. Wang Z, Fingas M, Page DS (1999) Oil spill identification. *J Chromatogr A* 843(1):369–411.
36. Yunker MB, et al. (2002) PAHs in the Fraser River basin: A critical appraisal of PAH ratios as indicators of PAH source and composition. *Org Geochem* 33(4):489–515.
37. Gustafsson Ö, Gschwend PM, Buesseler KO (1997) Using 234 Th disequilibria to estimate the vertical removal rates of polycyclic aromatic hydrocarbons from the surface ocean. *Mar Chem* 57(1):11–23.
38. Wang ZD, et al. (1999) Quantitative characterization of PAHs in burn residue and soot samples and differentiation of pyrogenic PAHs from petrogenic PAHs—The 1994 Mobile Burn Study. *Environ Sci Technol* 33(18):3100–3109.
39. Yan B, et al. (2005) Molecular tracers of saturated and polycyclic aromatic hydrocarbon inputs into Central Park Lake, New York City. *Environ Sci Technol* 39(18):7012–7019.
40. Reddy CM, et al. (2012) Composition and fate of gas and oil released to the water column during the *Deepwater Horizon* oil spill. *Proc Natl Acad Sci USA* 109(50):20229–20234.
41. Ryerson TB, et al. (2012) Chemical data quantify *Deepwater Horizon* hydrocarbon flow rate and environmental distribution. *Proc Natl Acad Sci USA* 109(50):20246–20253.
42. Valentine DL, et al. (2010) Propane respiration jump-starts microbial response to a deep oil spill. *Science* 330(6001):208–211.
43. Khadikar PV, Mandloi D, Bajaj AV, Joshi S (2003) QSAR study on solubility of alkanes in water and their partition coefficients in different solvent systems using PI index. *Bioorg Med Chem Lett* 13(3):419–422.
44. Puls W, Kühl H, Frohse A, König P (1995) Measurements of the suspended matter settling velocity in the German Bight (North Sea). *Dtsch Hydrogr Z* 47(4):259–276.
45. Migon C, Sandroni V, Marty J-C, Gasser B, Miquel J-C (2002) Transfer of atmospheric matter through the euphotic layer in the northwestern Mediterranean: Seasonal pattern and driving forces. *Deep Sea Res Part II* 49(11):2125–2141.
46. Payne JR, Clayton JR, Kirstein BE (2003) Oil/suspended particulate material interactions and sedimentation. *Spill Sci Technol Bull* 8(2):201–221.
47. Theodosi C, et al. (2013) Downward fluxes of elemental carbon, metals and polycyclic aromatic hydrocarbons in settling particles from the deep Ionian Sea (NESTOR site), Eastern Mediterranean. *Biogeosciences* 10(7):4449–4464.
48. Dachs J, Bayona JM, Fowler SW, Miquel J-C, Albaigés J (1996) Vertical fluxes of polycyclic aromatic hydrocarbons and organochlorine compounds in the western Alboran Sea (southwestern Mediterranean). *Mar Chem* 52(1):75–86.
49. Aeppli C, Reddy CM, Nelson RK, Kellermann MY, Valentine DL (2013) Recurrent oil sheens at the *Deepwater Horizon* disaster site fingerprinted with synthetic hydrocarbon drilling fluids. *Environ Sci Technol* 47(15):8211–8219.
50. Reddy CM, et al. (2007) Identification and quantification of alkene-based drilling fluids in crude oils by comprehensive two-dimensional gas chromatography with flame ionization detection. *J Chromatogr A* 1148(1):100–107.
51. Neff JM (2005) *Composition, Environmental Fates, and Biological Effect of Water Based Drilling Muds and Cuttings Discharged to the Marine Environment: A Synthesis and Annotated Bibliography* (Am Petrol Inst, Washington, DC).
52. Emam EA (2013) Modified activated carbon and bentonite used to adsorb petroleum hydrocarbons emulsified in aqueous solution. *Am J Environ Prot* 2(6):161–169.
53. Joung D, Shiller AM (2013) Trace element distributions in the water column near the Deepwater Horizon well blowout. *Environ Sci Technol* 47(5):2161–2168.
54. Schlumberger (2007) M-I Wate – 4.1 Sg Barite - Introducing a 4.1 SG grade of barite to significantly extend reserves of acceptable drilling grade barite: www.slb.com/%7E/media/Files/miswaco/product_sheets/m-i_wate_barite.ashx.
55. Eagle M, Paytan A, Arrigo KR, van Dijken G, Murray RW (2003) A comparison between excess barium and barite as indicators of carbon export. *Paleoceanography* 18(3):1021.
56. Gonneea ME, Paytan A (2006) Phase associations of barium in marine sediments. *Mar Chem* 100(1-2):124–135.
57. Lea DW, Spero HJ (1992) Experimental-determination of barium uptake in shells of the planktonic-foraminifera *Orbulina universa* at 22°C. *Geochim Cosmochim Acta* 56(7):2673–2680.
58. Hönisch B, et al. (2011) Planktic foraminifers as recorders of seawater Ba/Ca. *Mar Micropaleontol* 79(1):52–57.
59. Lira VF, et al. (2011) Effects of barium and cadmium on the population development of the marine nematode *Rhabditis* (*Pellioditis*) marina. *Mar Environ Res* 72(4):151–159.

60. Polonini HC, et al. (2014) Ecotoxicological studies of micro- and nanosized barium titanate on aquatic photosynthetic microorganisms. *Aquat Toxicol* 154:58–70.
61. Bouloubassi I, et al. (2006) PAH transport by sinking particles in the open Mediterranean Sea: A 1 year sediment trap study. *Mar Pollut Bull* 52(5):560–571.
62. Dachs J, Bayona JM, Raoux C, Albaigés J (1997) Spatial, vertical distribution and budget of polycyclic aromatic hydrocarbons in the western Mediterranean seawater. *Environ Sci Technol* 31(3):682–688.
63. Chanton JP, et al. (2012) Radiocarbon evidence that carbon from the *Deepwater Horizon* spill entered the planktonic food web of the Gulf of Mexico. *Environ Res Lett* 7(4):045303.
64. Boothe PN, Presley BJ (1989) Trends In sediment trace element concentrations around six petroleum drilling platforms in the northwestern Gulf of Mexico, Drilling Wastes. Proceedings of 1988 International Conference on Drilling Wastes, ed Engelhardt FR, Ray JP, Gilliam HH (Elsevier, New York), pp 3–22.
65. Gordon ES, Goni MA (2004) Controls on the distribution and accumulation of terrigenous organic matter in sediments from the Mississippi and Atchafalaya river margin. *Mar Chem* 92(1):331–352.
66. Gordon ES, Goñi MA (2003) Sources and distribution of terrigenous organic matter delivered by the Atchafalaya River to sediments in the northern Gulf of Mexico. *Geochim Cosmochim Acta* 67(13):2359–2375.
67. Goñi MA, Ruttenberg KC, Eglinton TI (1997) Sources and contribution of terrigenous organic carbon to surface sediments in the Gulf of Mexico. *Nature* 389(6648): 275–278.
68. Montagna PA, et al. (2013) Deep-sea benthic footprint of the *Deepwater Horizon* blowout. *PLoS One* 8(8):e70540.
69. Murawski SA, Hogarth WT, Peebles EB, Barbeiri L (2014) Prevalence of external skin lesions and polycyclic aromatic hydrocarbon concentrations in Gulf of Mexico fishes, post-*Deepwater Horizon*. *Trans Am Fish Soc* 143(4):1084–1097.
70. Fisher CR, et al. (2014) Footprint of *Deepwater Horizon* blowout impact to deepwater coral communities. *Proc Natl Acad Sci USA* 111(32):11744–11749.
71. White HK, et al. (2012) Impact of the *Deepwater Horizon* oil spill on a deep-water coral community in the Gulf of Mexico. *Proc Natl Acad Sci USA* 109(50):20303–20308.
72. Choi YH, Wang Y (2004) Dynamics of carbon sequestration in a coastal wetland using radiocarbon measurements. *Global Biogeochem Cycles* 18(4):GB4016.
73. Vogel JS, Southon JR, Nelson DE, Brown TA (1984) Performance of catalytically condensed carbon for use in accelerator mass-spectrometry. *Nucl Instrum Meth Phys Res B* 5(2):289–293.
74. Stuiver M, Polach HA (1977) Reporting of ^{14}C data. *Radiocarbon* 19(3):355–363.
75. McNichol AP, Aluwihare LI (2007) The power of radiocarbon in biogeochemical studies of the marine carbon cycle: Insights from studies of dissolved and particulate organic carbon (DOC and POC). *Chem Rev* 107(2):443–466.
76. Trumbore S (2009) Radiocarbon and soil carbon dynamics. *Annu Rev Earth Planet Sci* 37:47–66.
77. Brenna JT, Corso TN, Tobias HJ, Caimi RJ (1997) High-precision continuous-flow isotope ratio mass spectrometry. *Mass Spectrom Rev* 16(5):227–258, and erratum (1997) 16(6):382.
78. Fry B, Silva SR, Kendall C, Anderson RK (2002) Oxygen isotope corrections for online δ^{34}S analysis. *Rapid Commun Mass Spectrom* 16(9):854–858.
79. Coplen TB, Krouse HR (1998) Sulphur isotope data consistency improved. *Nature* 392(6671):32.
80. Utermöhl H (1958) Zur vervollkommnung der quantitativen phytoplankton-methodik. *Mitt Int Verh Limnol* 9:1–38.
81. Han YM, et al. (2009) The effect of acidification on the determination of elemental carbon, char-, and soot-elemental carbon in soils and sediments. *Chemosphere* 75(1): 92–99.
82. Han Y, et al. (2007) Evaluation of the thermal/optical reflectance method for quantification of elemental carbon in sediments. *Chemosphere* 69(4):526–533.
83. Chow JC, et al. (1993) The dri thermal/optical reflectance carbon analysis system: Description, evaluation and applications in U.S. Air quality studies. *Atmos Environ Part A* 27(8):1185–1201.
84. Louchouarn P, et al. (2007) Elemental and molecular evidence of soot- and char-derived black carbon inputs to New York City's atmosphere during the 20th century. *Environ Sci Technol* 41(1):82–87.
85. Gustafsson Ö, Haghseta F, Chan C, MacFarlane J, Gschwend PM (1996) Quantification of the dilute sedimentary soot phase: Implications for PAH speciation and bioavailability. *Environ Sci Technol* 31(1):203–209.
86. Han Y, et al. (2013) Thermal/optical methods for elemental carbon quantification in soils and urban dusts: Equivalence of different analysis protocols. *PLoS One* 8(12): e83462.
87. Han Y, et al. (2007) Evaluation of the thermal/optical reflectance method for discrimination between char- and soot-EC. *Chemosphere* 69(4):569–574.
88. Buist I, Trudel K, Morrison J, Aurand D (1997) Laboratory studies of the properties of in-situ burn residues. *Int Oil Spill Conf Proc* 1997(1):149–156.
89. Masiello CA (2004) New directions in black carbon organic geochemistry. *Mar Chem* 92(1):201–213.
90. Bray EE, Evans ED (1961) Distribution of N-paraffins as a clue to recognition of source beds. *Geochim Cosmochim Acta* 22(1):2–15.
91. Wakeham SG, Schaffner C, Giger W (1979) Polycyclic aromatic hydrocarbons in recent lake sediment I. Compounds having anthropogenic origins. *Geochim Cosmochim Acta* 44(3):403–413.
92. Sporstol S, et al. (1983) Source identification of aromatic hydrocarbons in sediments using GC/MS. *Environ Sci Technol* 17(5):282–286.
93. Yan B (2004) PAH sources and depositional history in sediments from the lower hudson river basin. Ph.D. dissertation (Rensselaer Polytech Inst, Troy, NY).
94. Lima AL, Eglinton TI, Reddy CM (2003) High-resolution record of pyrogenic polycyclic aromatic hydrocarbon deposition during the 20th century. *Environ Sci Technol* 37(1): 53–61.
95. Aeppli C, et al. (2014) Recalcitrance and degradation of petroleum biomarkers upon abiotic and biotic natural weathering of *Deepwater Horizon* oil. *Environ Sci Technol* 48(12):6726–6734.
96. Bence AE, Kvenvolden KA, Kennicutt MC (1996) Organic geochemistry applied to environmental assessments of Prince William Sound, Alaska, after the *Exxon Valdez* oil spill—A review. *Org Geochem* 24(1):7–42.
97. Fine PM, Cass GR, Simoneit BRT (2001) Chemical characterization of fine particle emissions from fireplace combustion of woods grown in the northeastern United States. *Environ Sci Technol* 35(13):2665–2675.
98. Overton EB, Miles MS, Meyer BM, Gao H, Turner RE (2014) Oil source fingerprinting in heavily weathered residues and coastal marsh samples. *Int Oil Spill Conf Proc* 2014(1):2074–2082.
99. Spear JW, Poore RZ (2011) *Seasonal Flux and Assemblage Composition of Planktic Foraminifera from the Northern Gulf of Mexico, 2008–2009* (U. S. Geol Surv, Boulder, CO).
100. Sternberg E, Tang D, Ho T-Y, Jeandel C, Morel FM (2005) Barium uptake and adsorption in diatoms. *Geochim Cosmochim Acta* 69(11):2745–2752.
101. Hughes I, Hase T (2010) *Measurements and Their Uncertainties: A Practical Guide to Modern Error Analysis* (Oxford Univ Press, New York).
102. Lipiatou E, et al. (1997) Mass budget and dynamics of polycyclic aromatic hydrocarbons in the Mediterranean Sea. *Deep Sea Res Part II* 44(3):881–905.
103. Adhikari PL, Maiti K, Overton EB (2015) Vertical fluxes of polycyclic aromatic hydrocarbons in the northern Gulf of Mexico. *Mar Chem* 168:60–68.